#### PHYSICAL REVIEW B 88, 174105 (2013)

### From parallel to single crystallization kinetics in high-density amorphous ice

Markus Seidl, Katrin Amann-Winkel, Philip H. Handle, Gerhard Zifferer, and Thomas Loerting 1,\*

1 Institute of Physical Chemistry, University of Innsbruck, Innrain 52a, A-6020 Innsbruck, Austria

2 Department of Physical Chemistry, University of Vienna, Währinger Straße 42, A-1090 Wien, Austria

(Received 7 December 2012; published 15 November 2013)

The isobaric transformation behavior of unannealed (uHDA) and expanded (eHDA) high-density amorphous ice at pressures up to 0.20 GPa is compared using powder x-ray diffraction and dilatometry. eHDA shows high thermal stability and crystallizes to a *single ice phase* only, whereas uHDA shows much lower thermal stability and always crystallizes to a *mixture of ice phases*. Unexpectedly, at low temperatures hexagonal ice grows first from uHDA, whereas this phase never crystallizes from eHDA. This leads us to conclude that hidden structural order in the form of nanocrystalline domains is present in uHDA, which triggers growth of hexagonal ice. By contrast, these ordered domains are absent in eHDA, which appears to be a homogeneous material and, thus, could be considered as a candidate for the low-temperature proxy of the proposed high-density liquid phase of water. The present work provides the basis for further experimental studies aiming at investigating this possibility since it establishes that the well-studied uHDA is not the right material to be studied in this context, whereas the more recently discovered eHDA is.

DOI: 10.1103/PhysRevB.88.174105 PACS number(s): 62.50.-p, 65.60.+a, 64.60.My

High-density amorphous ice (HDA) plays a key role in attempts of explaining the anomalous nature of water, especially in its supercooled state. 1-3 The nature of HDA has been a source of controversy since its discovery in 1984.<sup>4</sup> While Mishima et al. had suggested the pressure-induced amorphization of hexagonal ice (ice Ih) at  $\sim$ 80 K to be a "lowtemperature melting" resulting in glassy material (Lindemann transition), 4 others proposed it to be a mechanical collapse of the ice lattice accompanied by phonon softening and violation of the Born stability criteria of lattices.<sup>5-7</sup> Regardless of the formation mechanism considered, at 80 K and above  $\sim$ 1.1 GPa (which is the onset pressure for HDA formation at this temperature),<sup>4,8</sup> the amorphous state has a smaller Gibbs free energy. Otherwise, the transformation of ice Ih to HDA would not take place. While in the interpretation of the amorphization as "low-temperature melting" there is a thermodynamically continuous connection between HDA and high-pressure liquid water, there is none in the interpretation of the amorphization as mechanical collapse of the ice lattice. The former interpretation sees HDA as a continuous random structure of a glass, whereas the latter views HDA as being, e.g., composed of nanocrystals with a close resemblance of HDA and high-pressure ice polymorphs. 9-13 Distinguishing between the two options has been possible neither by diffraction nor by calorimetric methods. 11 The observation of a glass transition in HDA<sup>14–17</sup> would favor the former interpretation, but evidence for the glass transition in amorphous ice has traditionally been a subject of controversy. 18

Furthermore, a change of the amorphization mechanism from "thermal melting" at >162 K to "mechanical collapse" at <140 K has been inferred, with a smooth crossover of the mechanisms in between. This crossover has later been confirmed albeit with a lower crossover temperature around 100 K and constant pressure of mechanical collapse down to 30 K. HDA produced at high temperature is called expanded HDA (eHDA; cf. arrow labeled "Thermal Relaxation" in Fig. 1), 22.23 and HDA produced at ~80 K as proposed by Mishima *et al.* is called unannealed HDA (uHDA; cf.

arrow labeled "Mechanical Collapse" in Fig. 1) nowadays.<sup>22</sup> According to the result of the mechanistic crossover<sup>8,20,21</sup> one generally expects that uHDA and eHDA show qualitatively different structural features, i.e., not only quantitative differences (like the maximum of the first halo peak of x-ray powder diffractograms<sup>3</sup>) reflecting mainly the state of relaxation. We want to emphasize that the additional meaning of the term qualitatively (compared to the term quantitatively) is related to fundamentally different observations, i.e., the presence vs the absence of a structural feature. On the one hand, the oxygenoxygen radial distribution functions derived from neutron scattering experiments have so far been unable to resolve such structural differences between uHDA and eHDA.<sup>24</sup> On the other hand, a polarized Raman spectroscopic study probing the macroscopic network structure indicates that only uHDA is heterogeneous<sup>25</sup> and studies of the thermal stability at ambient pressure against transformation to low-density amorphous ice (LDA) reveal much lower transformation temperatures for uHDA compared to eHDA. 22,26–29 However, the Raman study shows that during annealing at a moderate pressure of 0.20 GPa, uHDA relaxes toward a more homogeneous structure similar to the one of eHDA<sup>25</sup> and, likewise, the lower thermal stability of uHDA compared to eHDA has been shown to vanish due to relaxation upon annealing of uHDA at the same pressure.<sup>27</sup> (A discussion of the actual pressure's role during annealing is given in the context of the present study's results below.) That is, since the state of relaxation is a quantitative measure only, the expected qualitatively different structural features of uHDA and eHDA are hidden with respect to the experiments on amorphous ices discussed so far.

Since crystallization is the formal reversal of the amorphization process, we consider the study of crystal growth to be most suitable to unveil this hidden difference. The crystallization of uHDA in the pressure range between 0.2 and 1.9 GPa has been studied by Salzmann *et al.*<sup>30</sup> The most surprising result in this study is that uHDA shows (at least) two crystallization modes and crystallizes at  $\leq 0.31$  GPa to ice Ih, whereas crystalline high-pressure phases of ice and all other amorphous ices

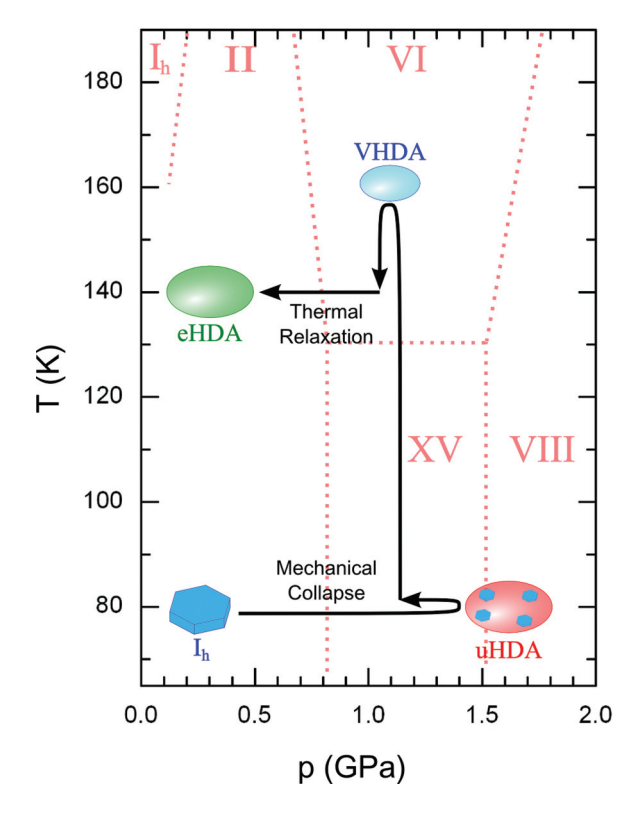


FIG. 1. (Color online) Schematic depiction of the pressure-temperature path taken to prepare uHDA and eHDA (via VHDA) from ice Ih on the background of the phase diagram. The color coding is used throughout the manuscript: uHDA (red) and eHDA (green). Ellipses represent amorphous ices and the size of the ellipses indicates their molar volumes; hexagonal prisms shown inside uHDA represent residual structural order after amorphization.

crystallize first to cubic ice (ice Ic).<sup>31</sup> They claim that it "is possible that ice Ih used for formation of HDA on pressure amorphizing at 77 K had not been completely converted." Hence, a detailed study of the crystallization behavior of both uHDA and eHDA may indeed reveal the expected qualitatively different structural features of these types of HDA that must have been hidden in the previous studies focusing on their comparison. <sup>22,25–29,32,33</sup> Therefore, we have conducted isobaric crystallization experiments using uHDA and eHDA, respectively, at several pressures up to 0.20 GPa here. uHDA is obtained by pressurizing ice Ih at  $\sim$ 80 K to 1.6 GPa (arrow labeled "Mechanical Collapse" in Fig. 1). eHDA is prepared by isobaric heating of that uHDA at 1.1 GPa to 160 K, leading to its transformation to very high-density amorphous ice (VHDA),<sup>34</sup> followed by isothermal decompression at 140 K to 0.20 GPa (arrow labeled "Thermal Relaxation" in Fig. 1)<sup>23</sup> and by quench recovery to  $\sim 80$  K. We emphasize that we have shown earlier that the quench-recovered phase represents the phase at high-temperature and high-pressure conditions since no irreversible changes of density occur in the course of quench recovery.<sup>35</sup> The main result of this work is that eHDA no longer exhibits the second mode of crystallization leading to hexagonal ice Ih. We discuss this finding as a result of residual structural order in uHDA, which apparently provides seeds for the growth of ice Ih.

Sample preparation and measurements were conducted with a piston cylinder apparatus with a bore of 8 mm and a computerized "universal testing machine" (Zwick, Model BZ100/TL3S). Pressure drops were avoided by lining the sample with indium foil.<sup>4,36</sup> Temperature measurement was realized using a temperature sensor (Pt-100) inserted firmly in the piston cylinder apparatus. For the crystallization experiments, all samples were brought to a pressure between 0.001 GPa (10 bar) and 0.20 GPa (2 kbar) at  $\sim$ 80 K and then heated to a certain temperature, applying a heating rate of 2 or 3 K/min. The isobaric heating curves are analyzed by following the volume change  $\Delta V$ , which is calculated by multiplying the piston displacement with the area of the cross section of the bore (further experimental details are given in Ref. 35). For each pressure, several heating experiments with different maximum temperatures were conducted. For all experiments, details on both the volume change and pressure evolution during isobaric heating are provided in Figs. SM1 and SM2 in the Supplemental Material, showing their good reproducibility.<sup>37</sup> Upon reaching the final temperature, the samples were quench recovered to ~80 K and subsequently decompressed to ambient pressure at that temperature. All recovered samples were characterized by x-ray powder diffraction at ~80 K and (sub)ambient pressure, using a diffractometer in  $\theta$ - $\theta$  geometry (Siemens, model D 5000,  $CuK\alpha$ ) equipped with a low-temperature camera from Paar.

In Fig. 2 the volume change  $\Delta V$  at 0.001 GPa (left column) and 0.10 GPa (right column) upon isobaric heating with a rate of 2 K/min are shown both for starting material uHDA (red dotted curves) and eHDA (green solid curves) in the top panels. Triangles indicate the temperatures from which the samples have been recovered before recording a powder diffractogram at  $\sim 80$  K (bottom panels of Fig. 2). For all pressures studied the linear thermal expansion up to  $\sim$ 120 K of uHDA (red dotted curves) is greater than that of eHDA (green solid curves). This observation reflects that samples of eHDA are well relaxed<sup>26</sup> while samples of uHDA are not and slowly relax<sup>38–40</sup> towards less dense amorphous structures. 22,27,35 We have chosen these two pressures because the transformation pathways are different: At 0.001 GPa an amorphous-amorphous transition to LDA is involved, and LDA is the material that then crystallizes. The transformation from HDA to LDA is evidenced by the shift of the broad halo maximum from  $\sim 31^{\circ}$  to  $\sim 24^{\circ}$  [see arrows in Figs. 2(b) and 2(c)]. At 0.10 GPa, however, HDA crystallizes without prior transformation to LDA. Additional experiments at 0.004 and 0.20 GPa are shown in Fig. SM3 in the Supplemental Material,<sup>37</sup> which show qualitatively the same behavior as at 0.001 and 0.10 GPa, respectively.

The powder x-ray diffractograms in the bottom panels in Fig. 2 (and in Fig. SM3 in the Supplemental Material<sup>37</sup>) demonstrate that eHDA remains entirely amorphous up to much higher temperatures than uHDA. This becomes particularly clear when comparing the diffractogram labeled 150 K (138 K) in Fig. 2(b) (Fig. 2(e)) with the diffractogram labeled 150 K (138 K) in Fig. 2(c) (Fig. 2(f)). Sharp Bragg reflections characteristic of ice Ih are evident only in case of uHDA as starting material, whereas in the case of eHDA as starting material there is no evidence for any sharp Bragg reflections. The onset crystallization temperature is found to be about 10 K

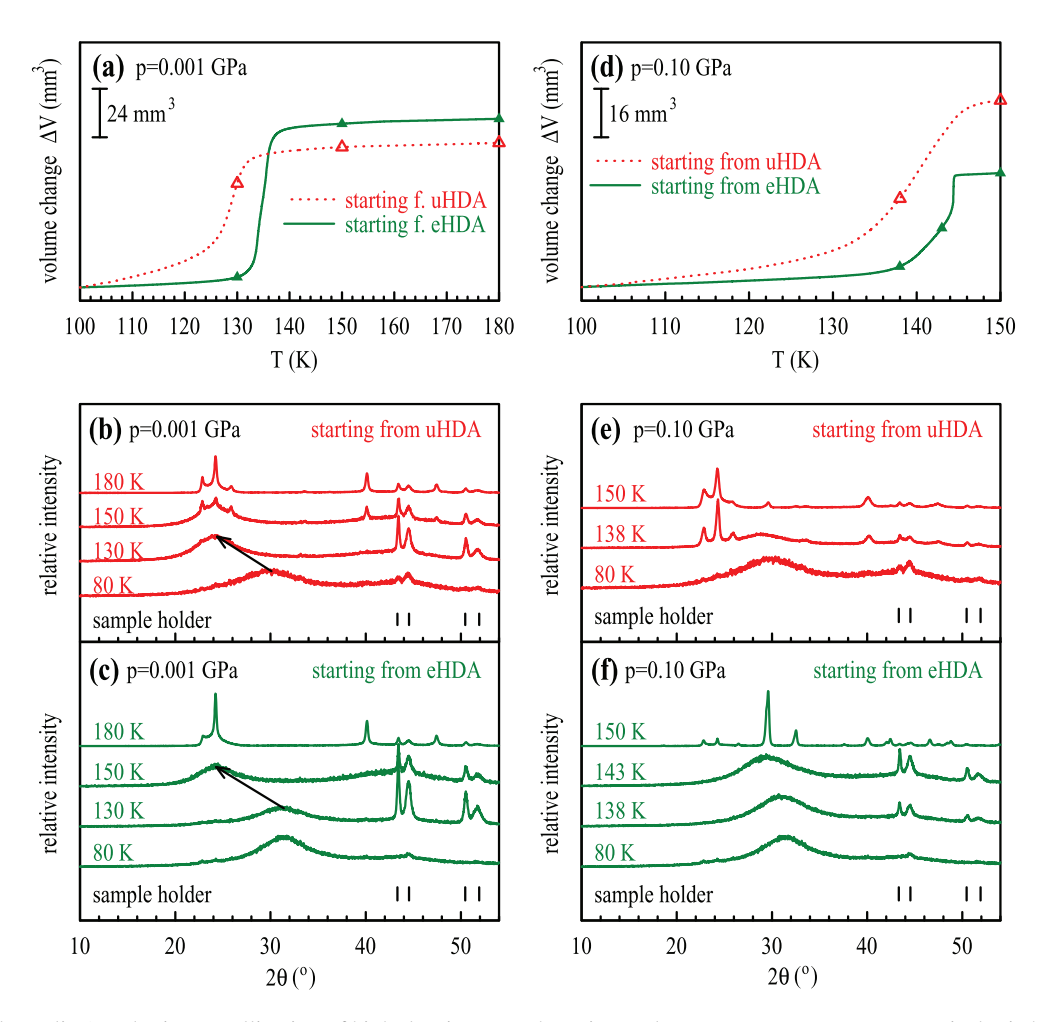


FIG. 2. (Color online) Isobaric crystallization of high-density amorphous ice. Volume-temperature curves upon isobaric heating (2 K/min) of uHDA (red dotted curve) and eHDA (green solid curve) are shown for 0.001 GPa (a) and 0.10 GPa (d). Triangles indicate the states for which powder diffractograms have been recorded. Corresponding diffractograms for samples recovered to  $\sim$ 80 K and (sub)ambient pressure are shown for both starting material uHDA (b), (e) and eHDA (c), (f). Curves are offset for clarity. Temperature labels indicate the maximum temperature experienced in isobaric heating runs and arrows mark the shift of halo peak maxima reflecting the transformation of HDA to LDA. The starting materials uHDA and eHDA, respectively, are characterized by a broad halo peak with a maximum at  $\sim$ 30.1° [(b) and (e)], and  $\sim$ 31.4° [(c) and (f)], respectively. The phase composition reads as follows: (b) HDA (80 K), LDA/trace ice Ih (130 K), LDA/ice Ih (150 K), ice Ih/ice Ic (180 K); (c) HDA (80 K), HDA/LDA (130 K), LDA (150 K), ice Ic (180 K); (e) HDA (80 K), HDA/ice Ih (138 K), ice Ih/ice IX (150 K); (f) HDA (80–143 K), ice IX/trace Ic (150 K).

higher for eHDA than for uHDA. Interestingly, when uHDA is heated ice Ih forms at the onset of crystallization, <sup>30</sup> whereas from Ostwald's step rule<sup>41</sup> one would expect metastable ice Ic to crystallize first. This is the case both at 0.001 GPa, where ice Ih appears in an LDA matrix at 150 K, and at 0.10 GPa, where ice Ih appears in an HDA matrix at 138 K. By contrast, when eHDA is heated spatially extended ice Ih does not appear at all in the temperature region studied. This is indicated by the absence of the characteristic hexagonal ice reflections at 25.9° (crystallographic [101] direction) and 33.6° ([102] direction) in Figs. 2(c) and 2(f). Hexagonal layers may only appear as two-dimensional stacking faults in spatially extended cubic ice, which is indicated by the appearance of the hexagonal [100] reflex at 23.0° in patterns of cubic ice. At 0.001 GPa (where the phase diagram shows ice Ih as the stable phase) first (metastable) LDA is produced, which then crystallizes to (less metastable) cubic ice—in full accordance with the expectations from Ostwald's step rule. At 0.10 GPa (where the phase diagram shows ice II as the stable phase; see Fig. 1) eHDA crystallizes directly to (metastable) ice IX. After complete crystallization the powder diffractograms in principle show a single phase: (stacking-faulty) cubic ice at 180 K and 0.001 GPa [Fig. 2(c)] and ice IX at 150 K and 0.10 GPa [Fig. 2(f)]. This demonstrates that eHDA shows a *single* mode of crystallization, whereas uHDA shows (at least) a *double* mode of crystallization. We emphasize that eHDA's transformation to a metastable phase is in accordance with the behavior expected for a glass. Alexant By contrast, e.g., a nanocrystalline material is supposed to transform to the stable phase. That is, our observation of eHDA's transformation to the metastable, and not the stable polymorph, thus favors the interpretation of it being glassy.

However, the mode of glass crystallization which leads to the metastable polymorph, namely ice Ic at 0.001 GPa and ice IX at 0.10 GPa, is also evident when starting from uHDA [Figs. 2(b) and 2(e)]: After a significant amount of hexagonal ice has grown, a second phase of ice starts to grow. In order to demonstrate the appearance of ice Ic after growth of ice Ih at 0.001 GPa from the diffractograms at 150 and 180 K [Fig. 2(b)] we follow the suggestion by Hansen et al. 45 and analyze the relative amount of ice Ih by forming the intensity ratio of the Bragg reflections at 25.9° (entirely due to hexagonal ice) and at 24.3° (due to both hexagonal and cubic ice). This ratio is zero when crystallizing from eHDA, i.e., it crystallizes to cubic ice containing some stacking faults, but does not show any signs of hexagonal ice growing in all three dimensions. When crystallizing from uHDA the intensity ratio is initially high, indicating crystallization of ice Ih in all three dimensions, and then drops significantly from 0.8 at 150 K to 0.2 at 180 K [Fig. 3(a)], indicating that crystallization of cubic ice at higher temperature lowers the relative amount of three-dimensional

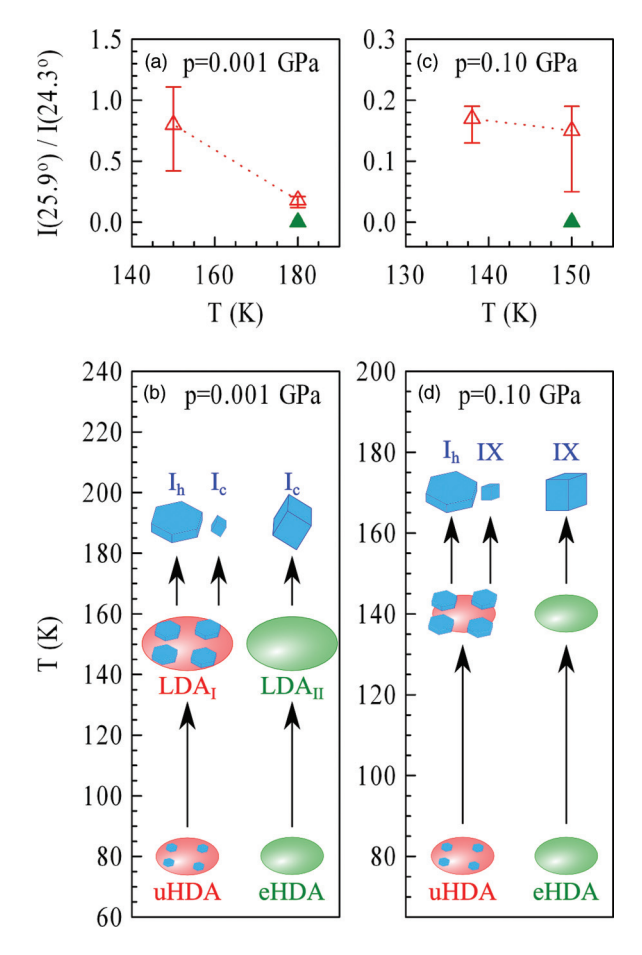


FIG. 3. (Color online) Parallel vs single crystallization kinetics in high-density amorphous ice. Analysis of the intensity ratio between two Bragg reflections to determine the relative amount of hexagonal vs cubic ice from the diffractograms in Fig. 1 for 0.001 GPa (a) and 0.10 GPa (c). Triangles indicate "most reasonable" values and error bars indicate the variation by considering ambiguities in the baseline. (b) and (d) show a sketch of the transformations experienced by uHDA (red) and eHDA (green) at 0.001 GPa and 0.10 GPa, respectively, as a function of temperature. Ellipses represent amorphous ices and the size of the ellipses indicates their molar volumes; hexagonal prisms shown inside uHDA represent residual structural order after amorphization.

ice Ih. At 0.10 GPa a significant decrease in hexagonal ice fraction [Fig. 3(c)] cannot be seen with increasing temperature from uHDA (since ice IX and not cubic ice crystallizes in the second mode), but nonzero values clearly indicate the presence of hexagonal ice.

Now, our observations allow us to clarify the nature of uHDA and eHDA at  $\sim$ 80 K, respectively, and to derive information on their topological differences. The presence of the crystallization mode to ice Ih in the case of uHDA and its absence in the case of eHDA suggests that there is in fact a qualitative difference between the structures of uHDA and eHDA, although x-ray and neutron diffraction barely show any difference between the two materials at ~80 K. According to these studies both materials are fully amorphous, without any signs of crystallinity.<sup>24</sup> Even though our experiments do not provide direct information on the structure of the types of HDA studied, we are aware of only one scenario able to explain all of our observations, which is described as follows: uHDA contains structural features (i.e., some kind of order) favoring growth of ice Ih, which are absent in eHDA. In principle, these features could be short-range-ordered domains, i.e., nanocrystals, as well as middle- or long-range correlations, i.e., mesoscaled structures. However, we rule out mesoscaled structures being responsible for the low-temperature growth of hexagonal ice and claim that they have to be on the nanometer length scale. While mesoscaled structures are annihilated by the polyamorphic transformation of uHDA to LDA, nanoscaled structures may remain unaffected by this transition, in which the macroscopic density and the global topology change dramatically. Furthermore, the individual ordered domains have to be smaller than ~2 nm according to a Rietveld analysis of neutron diffraction data on uHDA at 100 K.44 Also our x-ray instrument does not resolve any signs of order for uHDA at  $\sim$ 80 K [Figs. 2(b) and 2(e)]. That is, uHDA has to contain some nanocrystals, but it is not an entirely nanocrystalline material either. In fact, it is a heterogeneous system showing residual order from hexagonal ice in the form of nanocrystalline domains which are embedded in an amorphous matrix [Figs. 3(b) and 3(d)]. Even though the contact between an amorphous matrix and crystalline domains is thermodynamically unstable, such a system can sustain for many months provided the temperature is low enough,  $^{11}$  which is the case at  $\sim 80$  K. Upon heating uHDA the thermodynamically more stable ice Ih grows from the nanocrystals at the expense of the less stable amorphous matrix, representing one mode of crystal growth. In addition, our results show that the amorphous matrix itself starts to crystallize before it is consumed entirely by ice Ih, which represents another mode of crystal growth. As a result, uHDA crystallizes to a mixture of two ice phases. To conclude, our study confirms earlier indications that uHDA is not related to the structure of liquid water<sup>9,21</sup> because of the nanocrystalline domains favoring the growth of ice Ih.

In contrast, we here describe that in eHDA growth of ice Ih is no longer favored. That is, by following the *p-T* path labeled "Thermal Relaxation" in Fig. 1 it is possible to remove the residual structural order of uHDA, resulting in a purely glassy material. We emphasize that the key step leading to its removal is the annealing of uHDA at 1.1 GPa and 160 K, producing VHDA. Only under such high-pressure and high-temperature

conditions are the hexagonal nanocrystals thermodynamically less stable than the amorphous matrix. At 160 K hexagonal ice transforms to HDA at  $\sim 0.6$  GPa. That is, above  $\sim 0.6$  GPa the amorphous matrix HDA is thermodynamically more stable than hexagonal ice, but of course less stable than the stable high-pressure forms ice II and ice VI (see Fig. 1). At 1.1 GPa and 160 K nanocrystals of hexagonal ice will, therefore, completely transform to the glassy phase. As mentioned above, our results for uHDA heated at 0.20 GPa (data are shown in the Supplemental Material, Fig. SM3<sup>37</sup>) qualitatively correspond to those at 0.10 GPa, i.e., the nanocrystals do not transform to glassy material at this moderate pressure, but rather grow leading to a large amount of ice I after complete crystallization. By contrast, Suzuki and Tominaga reported that both annealing of uHDA at 0.20 and 1.5 GPa, respectively, result in a similar, homogeneous structure.<sup>25</sup> We explain this seeming contradiction by methodic differences: First, Raman spectroscopy probes relaxation of the macroscopic network structure, 25 while our experiments reveal the behavior of ordered domains on the nanometer length scale. Second, if "crystalline ices [...were] hidden in the unannealed HDA, [...] sharp and strong peaks relating to the crystalline phase should appear in the Raman spectra"25 upon annealing. Since such peaks are absent in their spectra of the uHDA relaxed at 0.20 GPa, they consider uHDA to be the low-temperature proxy of a liquid. We want to emphasize that the maximum temperature in their annealing procedure of 130 K lies below the onset temperature of crystal growth at 0.20 GPa [see Supplemental Material, Fig. SM3(e)<sup>37</sup>], and, thus, their claim does not hold. We assume that Suzuki and Tominaga would detect sharp peaks upon annealing, e.g., at 143 K [see Supplemental Material, Fig. SM3(e)<sup>37</sup>]. Our finding of glassy and, in this sense, homogeneous eHDA also seems to be contradictory to the scattering experiments at subambient pressure in which heterogeneity has been revealed for both uHDA and HDA-like states obtained by heating VHDA at ambient pressure. 32,33 It is unclear, though, what kind of structural features underlie the heterogeneities in these scattering experiments and whether or not these HDA-like states relate to eHDA.

We want to emphasize that our observation of two modes of crystallization in unrelaxed amorphous ice (uHDA) and one mode of crystallization in relaxed amorphous ice (eHDA) might be rationalized in terms of structural and dynamic heterogeneities. <sup>46</sup> It is conceivable that the water molecules move in a highly correlated way in strained or disturbed amorphous ices, giving rise to localized excitations. <sup>47,48</sup> Such

excitations may ultimately provide easy access to the crystallization channel to hexagonal ice Ih at rather low temperatures [e.g., <138 K at 0.10 GPa as shown in Fig. 2(e)], provided that Ih seeds are present and, thus, growth of nanocrystals is the dominant process rather than nucleation. It is evident from Figs. 3(b) and 3(d) that if there were no domains of hexagonal ice in the HDA matrix from the beginning, localized excitations would only be able to enhance nucleation and growth of metastable ices (e.g., at 0.10 GPa ice Ic and ice IX), as described by the Ostwald step rule. Actually, this situation is given in the case of eHDA. However, whereas the link between localized excitations was recently established in the context of the heterogeneous dynamics at the origin of the glass-toliquid transition, the actual link between such excitations and crystallization is much less clear. 47,48 It has been shown that mixtures of ices Ih and Ic may also grow from a homogeneous supercooled liquid,<sup>49</sup> but we regard this scenario to be unlikely in our case, because we also observe Ih and IX mixtures in our study. It seems highly unlikely that a mixture of two ices differing by about 20% in density might crystallize from a structurally homogeneous system. Simulations have shown that translational ordering and, thus, densification is indeed the initial step of the nucleation process in water.<sup>50</sup>

In this context and for the theoretical understanding of water in general it is crucial how much ordering liquid and glassy states, respectively, can have and still go on being liquids or the low-temperature proxies of liquids<sup>50–57</sup> (cf. the perspective article by Ediger and Harrowell<sup>58</sup>). The present work provides the basis for further experimental studies aiming at answering this key question since we show how to produce purely glassy HDA, which is the most realistic candidate for the proposed high-density liquid water<sup>59</sup> below the glass transition temperature. Our results explain why a link between uHDA and a liquid phase could not be found over the past 30 years,<sup>38</sup> while evidence for a glass-to-liquid transition was found for eHDA from ambient pressure<sup>17</sup> to 0.30 GPa<sup>16</sup> very soon after its recent discovery.<sup>23</sup>

#### **ACKNOWLEDGMENTS**

We thank David T. Limmer and David Chandler for discussion. Support by the European Research Council (ERC Starting Grant SULIWA to T.L.), the Austrian Science Fund (FWF START Award No. Y391 to T.L. and a Hertha-Firnberg fellowship to K.A.-W.), and the Austrian Academy of Sciences (DOC fellowship to M.S.) is gratefully acknowledged.

<sup>\*</sup>Telephone: 0043/512/507-5062; Email address: thomas.loerting@uibk.ac.at

<sup>&</sup>lt;sup>1</sup>P. G. Debenedetti, J. Phys.: Condens. Matter 15, R1669 (2003).

<sup>&</sup>lt;sup>2</sup>C. A. Angell, Annu. Rev. Phys. Chem. **55**, 559 (2004).

<sup>&</sup>lt;sup>3</sup>T. Loerting and N. Giovambattista, J. Phys.: Condens. Matter **18**, R919 (2006).

<sup>&</sup>lt;sup>4</sup>O. Mishima, L. D. Calvert, and E. Whalley, Nature **310**, 393 (1984). <sup>5</sup>J. S. Tse, J. Chem. Phys. **96**, 5482 (1992).

<sup>&</sup>lt;sup>6</sup>E. L. Gromnitskaya, O. V. Stal'gorova, A. G. Lyapin, V. V. Brazhkin, and O. B. Tarutin, JETP Lett. 78, 488 (2003).

<sup>&</sup>lt;sup>7</sup>T. Strässle, A. M. Saitta, S. Klotz, and M. Braden, Phys. Rev. Lett. **93**, 225901 (2004).

<sup>&</sup>lt;sup>8</sup>O. Mishima, Nature **384**, 546 (1996).

<sup>&</sup>lt;sup>9</sup>J. S. Tse and M. L. Klein, Phys. Rev. Lett. **58**, 1672 (1987).

<sup>&</sup>lt;sup>10</sup>M. Koza, H. Schober, A. Tölle, F. Fujara, and T. Hansen, Nature 397, 660 (1999).

<sup>&</sup>lt;sup>11</sup>G. P. Johari, Phys. Chem. Chem. Phys. **2**, 1567 (2000).

<sup>&</sup>lt;sup>12</sup>A. M. Saitta and F. Datchi, Phys. Rev. E **67**, 020201 (2003).

<sup>&</sup>lt;sup>13</sup>T. Loerting, V. V. Brazhkin, and T. Morishita, Adv. Chem. Phys. 143, 29 (2009).

- <sup>14</sup>O. Mishima, J. Chem. Phys. **121**, 3161 (2004).
- <sup>15</sup>O. Andersson, Proc. Natl. Acad. Sci. USA **108**, 11013 (2011).
- <sup>16</sup>M. Seidl, M. S. Elsaesser, K. Winkel, G. Zifferer, E. Mayer, and T. Loerting, Phys. Rev. B **83**, 100201 (2011).
- <sup>17</sup>K. Amann-Winkel, C. Gainaru, P. H. Handle, M. Seidl, H. Nelson, R. Böhmer, and T. Loerting, Proc. Natl. Acad. Sci. USA 110, 17720 (2013).
- <sup>18</sup>S. Capaccioli and K. L. Ngai, J. Chem. Phys. **135**, 104504 (2011).
- <sup>19</sup>J. S. Tse, D. D. Klug, C. A. Tulk, I. Swainson, E. C. Svensson, C. K. Loong, V. Shpakov, V. R. Belosludov, R. V. Belosludov, and Y. Kawazoe, Nature 400, 647 (1999).
- <sup>20</sup>T. Strässle, S. Klotz, G. Hamel, M. M. Koza, and H. Schober, Phys. Rev. Lett. **99**, 175501 (2007).
- <sup>21</sup>T. Strässle, A. Caviezel, B. Padmanabhan, V. Y. Pomjakushin, and S. Klotz, Phys. Rev. B 82, 094103 (2010).
- <sup>22</sup>R. J. Nelmes, J. S. Loveday, T. Straessle, C. L. Bull, M. Guthrie, G. Hamel, and S. Klotz, Nat. Phys. 2, 414 (2006).
- <sup>23</sup>K. Winkel, M. S. Elsaesser, E. Mayer, and T. Loerting, J. Chem. Phys. **128**, 044510 (2008).
- <sup>24</sup>T. Loerting, K. Winkel, M. Seidl, M. Bauer, C. Mitterdorfer, P. H. Handle, C. G. Salzmann, E. Mayer, J. L. Finney, and D. T. Bowron, Phys. Chem. Chem. Phys. 13, 8783 (2011).
- <sup>25</sup>Y. Suzuki and Y. Tominaga, J. Chem. Phys. **133**, 164508 (2010).
- <sup>26</sup>K. Winkel, E. Mayer, and T. Loerting, J. Phys. Chem. B **115**, 14141 (2011).
- <sup>27</sup>P. H. Handle, M. Seidl, and T. Loerting, Phys. Rev. Lett. **108**, 225901 (2012).
- <sup>28</sup> K. Amann-Winkel, F. Löw, P. H. Handle, W. Knoll, J. Peters, B. Geil, F. Fujara, and T. Loerting, Phys. Chem. Chem. Phys. 14, 16386 (2012).
- <sup>29</sup>F. Löw, K. Amann-Winkel, B. Geil, T. Loerting, C. Wittich, and F. Fujara, Phys. Chem. Chem. Phys. **15**, 576 (2013).
- <sup>30</sup>C. G. Salzmann, E. Mayer, and A. Hallbrucker, Phys. Chem. Chem. Phys. 6, 5156 (2004).
- <sup>31</sup>Y. P. Handa, D. D. Klug, and E. Whalley, Can. J. Chem. **66**, 919 (1988).
- <sup>32</sup>M. M. Koza, B. Geil, K. Winkel, C. Köhler, F. Czeschka, M. Scheuermann, H. Schober, and T. Hansen, Phys. Rev. Lett. 94, 125506 (2005).
- <sup>33</sup>M. M. Koza, T. Hansen, R. P. May, and H. Schober, J. Non-Cryst. Solids 352, 4988 (2006).
- <sup>34</sup>T. Loerting, C. Salzmann, I. Kohl, E. Mayer, and A. Hallbrucker, Phys. Chem. Chem. Phys. 3, 5355 (2001).
- <sup>35</sup>C. G. Salzmann, T. Loerting, S. Klotz, P. W. Mirwald, A. Hallbrucker, and E. Mayer, Phys. Chem. Chem. Phys. 8, 386 (2006).

- <sup>36</sup>I. Kohl, E. Mayer, and A. Hallbrucker, Phys. Chem. Chem. Phys. **3**, 602 (2001).
- <sup>37</sup>See Supplemental Material at http://link.aps.org/supplemental/ 10.1103/PhysRevB.88.174105 for detailed information on the reproducibility of the experiments for all pressures studied as well as additional data.
- <sup>38</sup>Y. P. Handa, O. Mishima, and E. Whalley, J. Chem. Phys. **84**, 2766 (1986).
- <sup>39</sup>E. L. Gromnitskaya, O. V. Stal'gorova, V. V. Brazhkin, and A. G. Lyapin, Phys. Rev. B **64**, 094205 (2001).
- <sup>40</sup>C. A. Tulk, C. J. Benmore, J. Urquidi, D. D. Klug, J. Neuefeind, B. Tomberli, and P. A. Egelstaff, Science 297, 1320 (2002).
- <sup>41</sup>W. Ostwald, Z. Phys. Chem. **22**, 289 (1897).
- <sup>42</sup>S. R. Elliott, *Physics of Amorphous Materials* (Longman Group Ltd., New York, 1983).
- <sup>43</sup>R. Zallen, *The Physics of Amorphous Solids* (John Wiley & Sons, Inc., New York, 1983).
- <sup>44</sup>S. Klotz, T. Straessle, A. M. Saitta, G. Rousse, G. Hamel, R. J. Nelmes, J. S. Loveday, and M. Guthrie, J. Phys.: Condens. Matter 17, S967 (2005).
- <sup>45</sup>T. C. Hansen, M. M. Koza, and W. F. Kuhs, J. Phys.: Condens. Matter 20, 285104 (2008).
- <sup>46</sup>P. Kumar, S. V. Buldyrev, S. R. Becker, P. H. Poole, F. W. Starr, and H. E. Stanley, Proc. Natl. Acad. Sci. USA 104, 9575 (2007).
- <sup>47</sup>A. S. Keys, J. P. Garrahan, and D. Chandler, Proc. Natl. Acad. Sci. USA **110**, 4482 (2013).
- <sup>48</sup>A. S. Keys, L. O. Hedges, J. P. Garrahan, S. C. Glotzer, and D. Chandler, Phys. Rev. X 1, 021013 (2011).
- <sup>49</sup>T. Li, D. Donadio, G. Russo, and G. Galli, Phys. Chem. Chem. Phys. **13**, 19807 (2011).
- <sup>50</sup>J. Russo and H. Tanaka, arXiv:1308.4231 [cond-mat.soft] (2013).
- <sup>51</sup>Y. Liu, A. Z. Panagiotopoulos, and P. G. Debenedetti, J. Chem. Phys. **131**, 104508 (2009).
- <sup>52</sup>E. B. Moore and V. Molinero, Nature **479**, 506 (2011).
- <sup>53</sup>D. T. Limmer and D. Chandler, J. Chem. Phys. **135**, 134503 (2011).
- <sup>54</sup>P. H. Poole, S. R. Becker, F. Sciortino, and F. W. Starr, J. Phys. Chem. B **115**, 14176 (2011).
- <sup>55</sup>F. Sciortino, I. Saika-Voivod, and P. H. Poole, Phys. Chem. Chem. Phys. **13**, 19759 (2011).
- <sup>56</sup>T. A. Kesselring, G. Franzese, S. V. Buldyrev, H. J. Herrmann, and H. E. Stanley, Sci. Rep. 2, 474 (2012).
- <sup>57</sup>P. H. Poole, R. K. Bowles, I. Saika-Voivod, and F. Sciortino, J. Chem. Phys. **138**, 034505 (2013).
- <sup>58</sup>M. D. Ediger and P. Harrowell, J. Chem. Phys. **137**, 080901
- <sup>59</sup>P. H. Poole, F. Sciortino, U. Essmann, and H. E. Stanley, Nature 360, 324 (1992).

## **Supplemental Material:**

# From parallel to single crystallization kinetics in high-density amorphous ice

Markus Seidl, <sup>a</sup> Katrin Amann-Winkel, <sup>a</sup> Philip H. Handle, <sup>a</sup> Gerhard Zifferer, <sup>b</sup> Thomas Loerting <sup>a,\*</sup>

<sup>a</sup>Institute of Physical Chemistry, University of Innsbruck, Innrain 52a, A-6020 Innsbruck, Austria
 <sup>b</sup>Department of Physical Chemistry, University of Vienna, Währinger Str. 42, A-1090 Wien, Austria

e-mail: <a href="mailto:thomas.loerting@uibk.ac.at">thomas.loerting@uibk.ac.at</a>
phone: 0043/512/507-5062

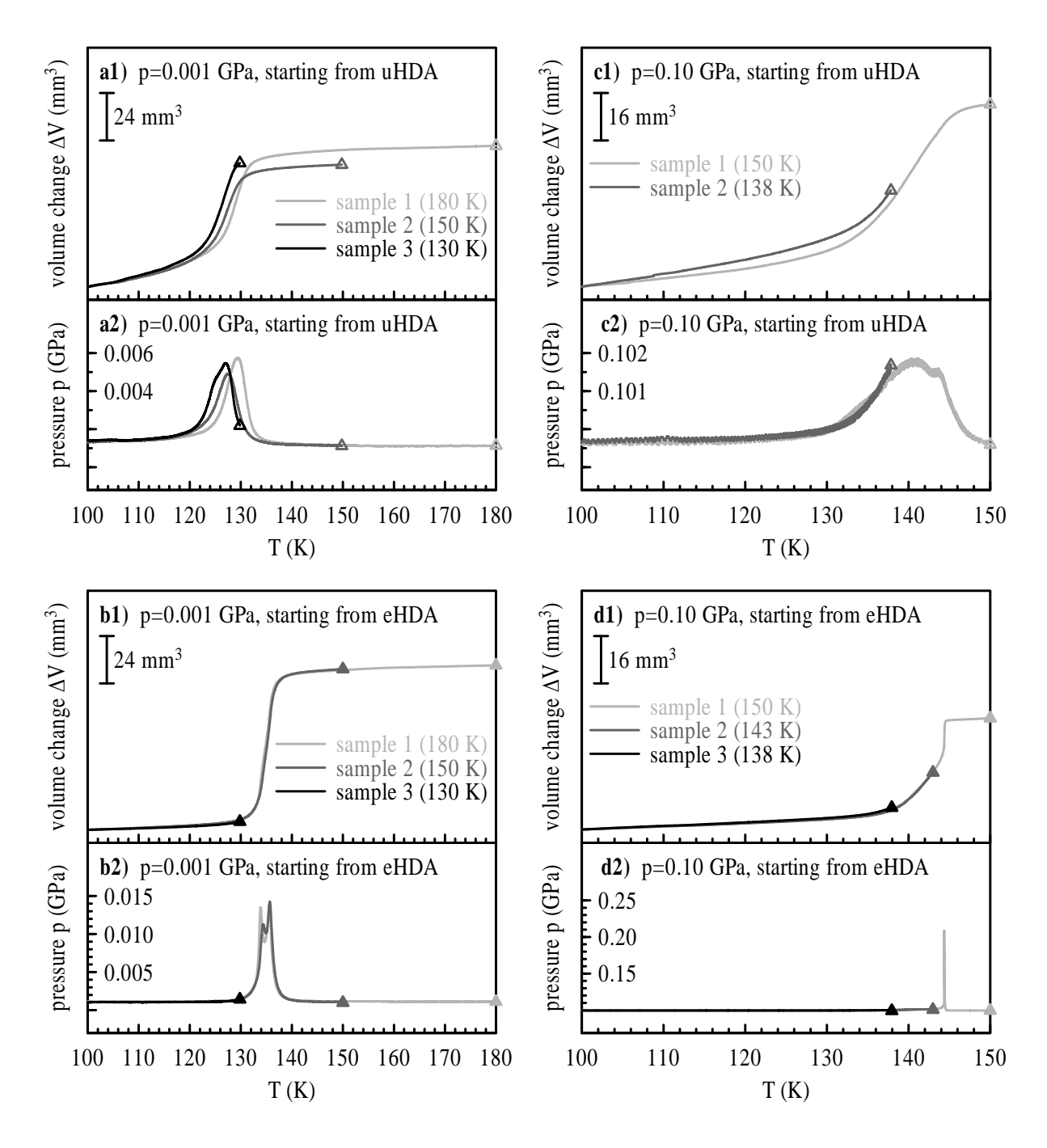


FIG. SM1. Reproducibility of the volume change and pressure evolution during isobaric heating of high-density amorphous ices at 0.001 GPa (left column) and 0.10 GPa (right column). The two or three distinct samples were prepared to gain powder diffractograms for states reached upon heating to different maximum temperatures (see Fig. 2, bottom panels). Triangles mark the end points of the curves, i.e. they indicate the states at the respective maximum temperatures (which are numerically given in the legend). In some cases the actual pressure significantly deviates from the nominal pressure in the temperature range where phase transformations take place (a2, b2 and d2). However, the phase behavior is governed by the pressure at the very onset of the transformation and, thus, the deviations at higher temperatures have no qualitative impact on the results.

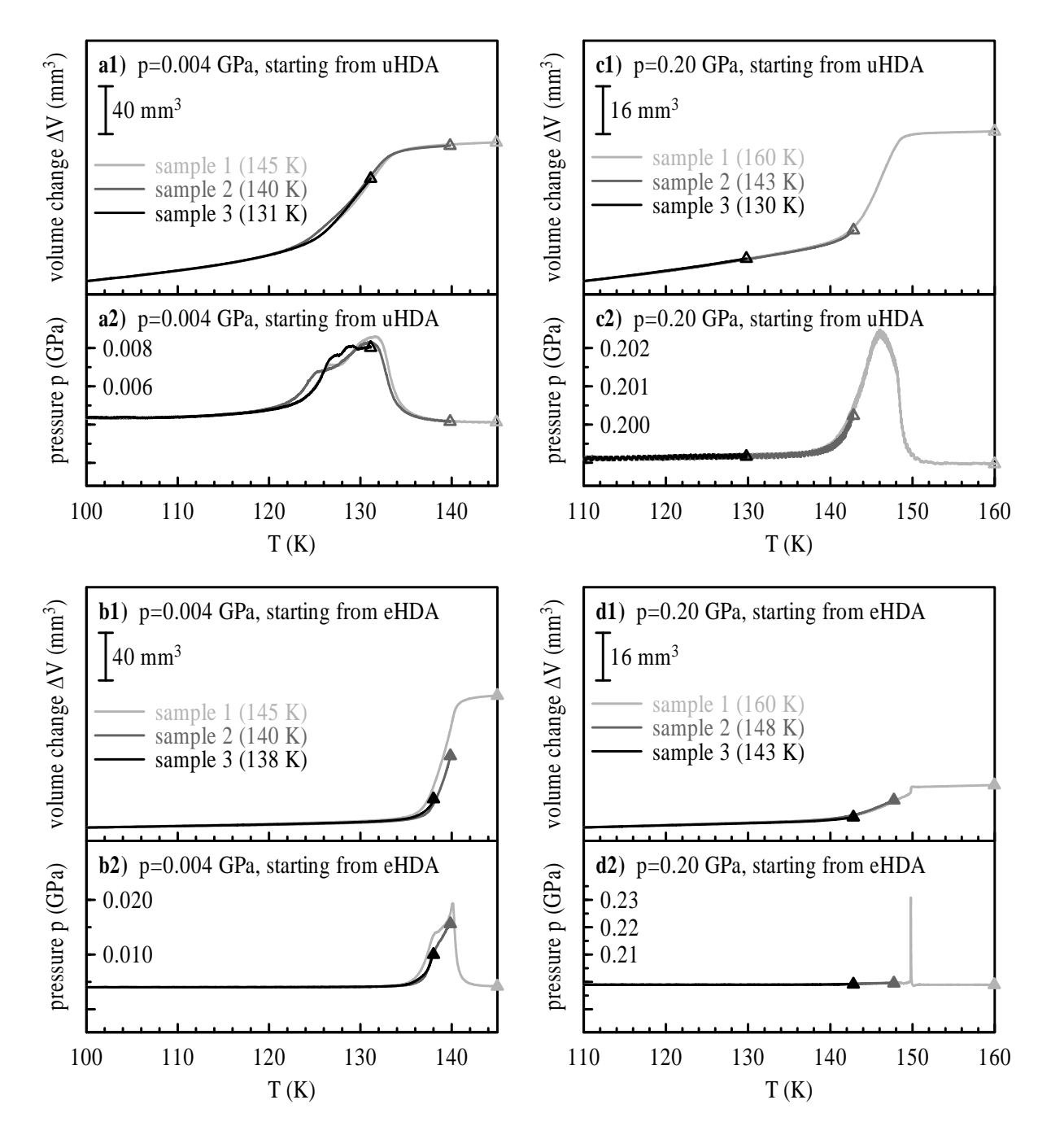


FIG. SM2. Reproducibility of the volume change and pressure evolution during isobaric heating of high-density amorphous ices at 0.004 GPa (left column) and 0.20 GPa (right column). The three distinct samples were prepared to gain powder diffractograms for states reached upon heating to different maximum temperatures (see Fig. SM2, bottom panels). Triangles mark the end points of the curves, i.e. they indicate the states at the respective maximum temperatures (which are numerically given in the legend). In some cases the actual pressure significantly deviates from the nominal pressure in the temperature range where phase transformations take place (a2 and b2). However, the phase behavior is governed by the pressure at the very onset of the transformation and, thus, the deviations at higher temperatures have no qualitative impact on the results.

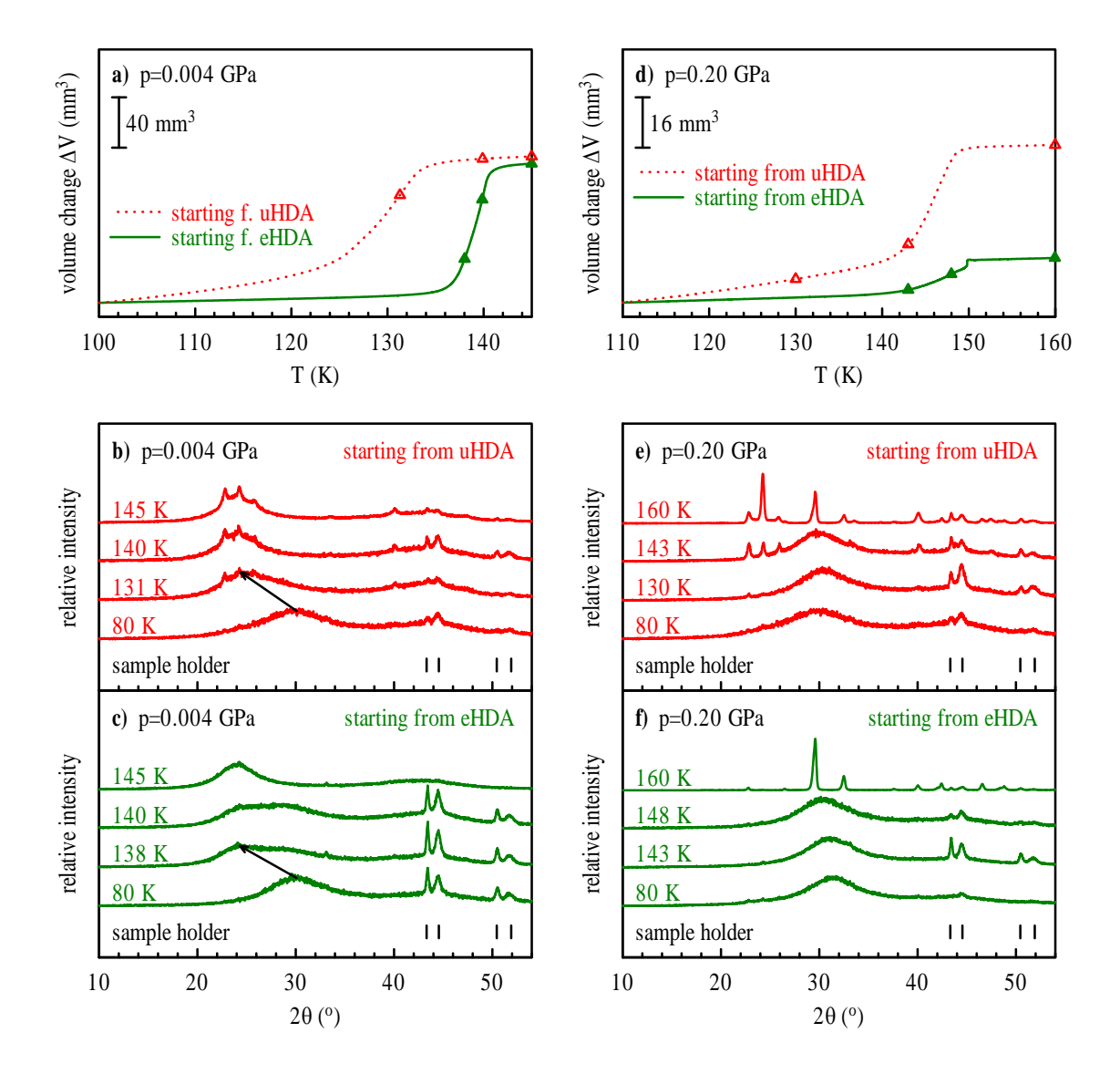


FIG. SM3. Isobaric crystallization of high-density amorphous ice. Volume-temperature curves upon isobaric heating of uHDA (red dotted curve) and eHDA (green solid curve) are shown for 0.004 GPa and 3 K/min (a) and 0.20 GPa and 2 K/min (d). Triangles indicate the states for which powder diffractograms have been recorded. Corresponding diffractograms for samples recovered to ~80 K and (sub)ambient pressure are shown for both starting material uHDA (b, e) and eHDA (c, f). Curves are offset for clarity. Temperature labels indicate the maximum temperature experienced in isobaric heating runs and arrows mark the shift of halo peak maxima reflecting the transformation of HDA to LDA. The starting material uHDA is characterized by a broad halo peak with a maximum at ~30.1° (panels (b) and (e)), while the starting material eHDA shows a peak maximum at ~30.1° (panel (c)) and ~31.4° (panel (f)), respectively. The phase composition reads as follows: (b) HDA (80 K), LDA/HDA/ice Ih (131 K), LDA/ice Ih (140–145 K); (c) HDA (80K), HDA/LDA (138–140 K), LDA (145 K); (e) HDA (80 K), HDA/ice Ih (143 K), ice IX/ice I (160K); (f) HDA (80–148 K), ice IX (160 K). In the case of 0.004 GPa uHDA was prepared by compression of ice Ih to 1.7 GPa at ~80 K and eHDA by decompression of VHDA to 0.10 GPa at 140 K. In the case of 0.20 GPa uHDA was prepared by compression of ice Ih to 1.6 GPa at ~80 K and eHDA by decompression of VHDA to 0.20 GPa at 140 K.